Mohamed et al. 2019. *Int. J. Vehicle Structures & Systems*, 11(1), 88-101
ISSN: 0975-3060 (Print), 0975-3540 (Online)
doi: 10.4273/ijvss.11.1.17

International Journal of Vehicle Structures & Systems
Available online at www.maftree.org/eja

Analysis of Synchronous Moment for Active Front Steering and a Two Actuated Wheels of Electric Vehicle Based on Dynamic Stability Enhancement

Eid S. Mohamed[a], Mohamed I. Khalil[b] and Ahmed A.A. Saad[b]

[a]*Mech. Engg. Dept. , Albaha University, KSA, on leave from Dept. of Automotive and Tractors Engg., Mataria, Helwan University, Cairo, Egypt. Corresponding Author, Email: eng_eid74@yahoo.com*
[b]*Automotive Engg. Dept., Helwan University, Cairo, Egypt*

ABSTRACT:

Active Front Steering (AFS) and Direct Yaw moment Controller (DYC) are the vehicle smart systems to improve the vehicle stability and safety. The AFS uses front wheels Steer-By-Wire (SBW) system. DYC uses Rear Independent in Wheel Actuated Electric Vehicles (RIWA-EVs). It generates yaw moment to correct the vehicle state deviations. The proposed controller algorithm consists of two levels. First level feedback controller evaluates the optimal yaw moment generated to achieve the desired vehicle trajectory motion with minimize the yaw rate and side-slip errors. The second level controller is utilized to allocate the required front steer angle and traction/ regeneration to the RIWA embedded in rear wheels by taking into account the tire slip. An optimal Linear Quadratic Regulator (LQR) controller is designed, and its controller effectiveness is evaluated under various input driving manoeuvres. The results indicate that the integrated AFS/DYC can significantly stabilize the vehicle motion and highly reduce the driver's workload. The laboratory experiment of AFS subsystem, for adequate actual front steering angle is measured, in order to apply in vehicle model to predict the responses. The results disclose that the RMS can be an effective route to monitor the vehicle stability.

KEYWORDS:

Vehicle motion stability; In-wheel actuated electric vehicle; Steering systems; Optimal LQR control

CITATION:

E.S. Mohamed, M.I. Khalil and A.A.A. Saad. 2019. Analysis of Synchronous Moment for Active Front Steering and a Two Actuated Wheels of Electric Vehicle Based on Dynamic Stability Enhancement, *Int. J. Vehicle Structures & Systems*, 11(1), 88-101. doi:10.4273/ijvss.11.1.17.

1. Introduction

Recently, the increasing concern over the environmental impact of the internal combustion engine vehicles (ICEVs), together with the soaring of oil prices, has led to a renewed interest in electric vehicles (EVs) [1]. The use of separate traction actuators at each wheel implies that torque to each drive wheel can be controlled independently. The performance of RIWA-EVs is likely to perform better compared with that of classical vehicles once a good control system is invented [2]. EVs utilize in-wheel motors to drive the wheels such that the torque of each wheel can be controlled independently. Such a flexible actuation can be easily used to generate the external yaw moment with the torque differences between the left and right wheels. Drive-by-wire and SBW control are designed and implemented in an EV. Such a feature has been exploited to devise a DYC to improve the vehicle's handling stability and performance [3-6]. On the other hand, Vehicle Dynamics Control (VDC) systems such as Active Steering Control (ASC) and DYC can certainly improve the handling performance of vehicle but in certain tire-working regions. ASC which includes AFS or Active Rear Steering (ARS) or Active Four-Wheel Steering (AFWS), can effectively improve the steer-ability performance of the vehicle [7].

Lateral stability of VDC is a very important aspect of improving vehicle stability and safety performance. A great deal of research on vehicle lateral dynamics stability control, including DYC or AFS control with SBW system, has been done in recent years [8-10]. AFS eliminates the mechanical steering column. In so doing, many traditional constraints are eliminated. Several works have been undertaken to study the control of vehicle handling using SBW system. AFS changes the tire lateral force to enhance the vehicle stability and DYC ensures the vehicle stability by controlling the tire longitudinal force. Because of the tire force saturation restriction, AFS stability control on vehicles is weaker than DYC, but AFS is better than the DYC in ride comfort. Vehicle AFS and DYC integrated control has been one of the chassis integrated control important research [11-12]. A reference model provides the desired yaw rate and body-slip angle based on driver's steering angle. Then a model matching controller or an optimal controller computes the yaw moment needed to make the actual handling to follow the reference model [13-16].

In DYC, the additional yaw moment is generated as a result of the difference in driving or braking forces between the right and left in-wheel actuators, or the Limited Slip Control Differential (LSCD). The DYC is considered as a way of controlling the lateral motion of a vehicle during a severe driving manoeuvre, Active Rear

Steer (ARS) as a four-Wheel Steering system (4WS) has been studied extensively in the field of vehicle motion control [17-20]. In this paper, a vehicle stability system using the rear 2-wheels motorized EV and AFS is proposed. A control algorithm is suggested to compensate for the error of the sideslip angle and the yaw rate by generating the DYC and AFS yaw moment. The test rig was built up to evaluate the AFS by SBW response in order to be applied in vehicle model to predict the responses.

2. AFS subsystem model

2.1. Principles of AFS system

The AFS system, Fig. 1(a), has the advantage of the absence of interference between the steering by the driver and the control of stability using the automatic front-wheel steering control because no mechanical linkage exists between the steering wheel (SW) and the steering gear. The steering by the driver is detected by a steering angle and torque sensors. This information is passed to a controller. The controller decision is passed to a steering actuator [21].

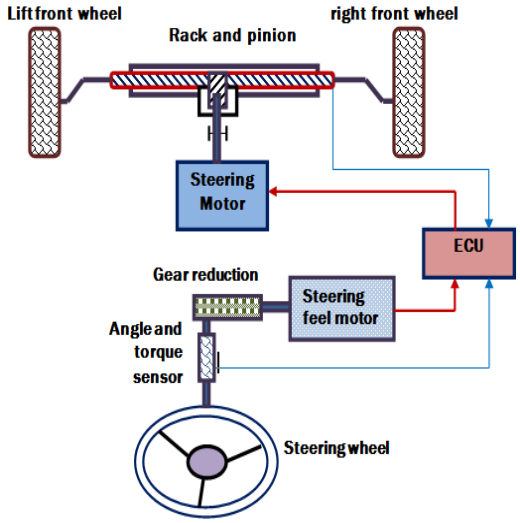

Fig. 1(a): Schematic diagram and model of AFS structure

2.2. Steering wheel (SW) model

The SW subsystem consists of a steering wheel, a steering column, a steering angle sensor, a torque sensor, a reducer, a road feeling motor and a road feeling motor driver. The steering angle and torque sensors are installed in the middle of steering column to sense the steering signals. Fig. 1(b) shows the SW system structure.

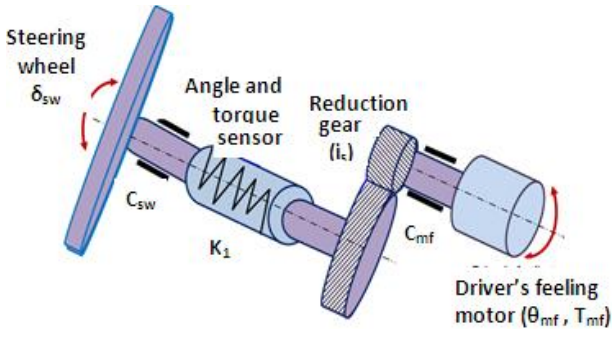

Fig. 1(b): Schematic diagram of wheel sub-system model

The dynamic model for SW is expressed by,

$$T_{sw} = J_{sw}\ddot{\delta}_{sw} + c_{sw}\dot{\delta}_d + K_1\left(\delta_{sw} - \frac{\theta_{mf}}{i_s}\right) \quad (1)$$

$$T_{mf} = J_{mf}\ddot{\theta}_{mf} + c_{mf}\dot{\theta}_{mf} + K_1\left(\theta_{mf} - i_s\delta_{sw}\right) \quad (2)$$

Where T_{sw} is the input torque of the SW, δ_{sw} is the angle of the SW. T_{mf} is the torque of the road feeling motor. J_{sw}, J_{mf} are the moment inertia of the SW and the road feeling motor. C_{sw}, C_{mf} are the damping co-efficient of the SW and the road feeling motor. K_1 represents the torsional stiffness of the column. i_s is the reduction ratio.

2.3. Road wheel (RW) model

The steering executive system is constituted of a driving motor, a rack-pinion gear, a reducer, an angle senor and the driving motor driver. The driving motor is installed at the rack mechanism, the structure of the steering executing system for the AFS system is shown in Fig. 1(c). The equations of motion in RW are as follows:

$$T_{md} = J_{md}\ddot{\theta}_{md} + C_{md}\dot{\theta}_{md} + K_r\left((\theta_{md}/i_d) - (X_r/r_p)\right)i_d^2 - M_a \quad (3)$$

The steering gear forces are expressed as,

$$m_r\ddot{X}_r = C_r\dot{X}_r + K_r\left((\theta_{md}/i_d) - (X_r/r_p)\right)i_d^2/r_p - F_L - F_R \quad (4)$$

The electric balance function of driving motor is,

$$U_{md} = R_{md}i(t) + L_{md}\dot{i} + K_{md}\dot{\theta}_{md}\; T_{md} = K_{emd}i \quad (5)$$

Where T_{md} is the torques of driving motor, F_L, F_R are the pinion force of the left/right wheels, i_d the represents the ratio of the reducer, r_p is the pinion radius, m_r is the pinion mass, C_{md} is the damping co-efficient of the rack. R_{md} is the resistance of the road feeling motor, L_{md} is the inductance of executive motor. The left/right tire aligning moments are M_a. The parameters of the AFS system and the vehicle are listed in Table 1. The AFS models and the control theory require models to be represented state motor actuator gain in linear state-space form.

Table 1: Main parameters of AFS model

Parameter	Symbols	Unit	Value
Mass moment of inertia of the motor armature	J_{md}	$kg.m^2$	0.0004
DC motor armature resistance	R_{md}	Ω	0.39
Motor armature inductance	L_{md}	H	0.0019
Torque constant of the motor	K_{emd}	$N.m/A$	0.052
Motor back EMF constant	K_{md}	$V/rad/s$	0.0521
Motor viscous damping coefficient	C_{md}	$N.m/rad/s$	0.19
Moment of inertia of steering wheel	J_{sw}	$N\ m\ s^2/rad$	0.0344
motor gear ratio	i_d	--	49/3
Viscous damping of feeling motor and steering wheel	C_{sw}	$N.m/rad/s$	0.3604
torsional stiffness of the column	K_1	$N\ cm\ /rad$	42057
Pinion radius	r_p	mm	20.75
Stiffness of Pinion	k_r	$N\ m\ /rad$	42057
Pinion mass	m_r	kg	0.26

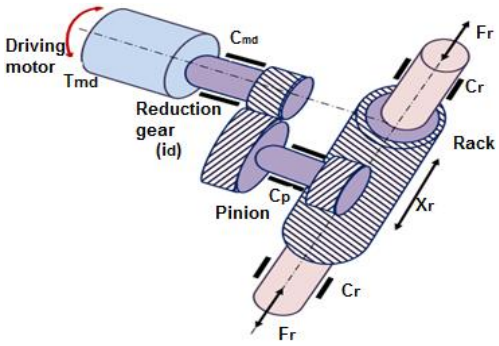

Fig. 1(c): Schematic diagram of executing sub-system

2.4. AFS angle model and AFS corrective yaw moment

The active steering angle δ_{AFS} which is required to increase or decrease the vehicle front steering wheel angle (SWA) is proposed as the following the corrective steering angle of front road wheels to be small, the corrective yaw moment of AFS is obtained as:

$$M_{z,AFS} = a\hat{C}_{\alpha f}\,\delta_C$$

Where $\hat{C}_{\alpha f}$ is the local lateral tire stiffness of two front wheels, defined as slope of total lateral front tire force with respect to the front tire slip angles using,

$$\hat{C}_{\alpha f} = \frac{\partial F_{yf}}{\partial \alpha_{\alpha f}}$$

The AFS angle is $\delta_{\text{AFS}} = \delta_c + \delta_{sw}$ Where δ_{sw} is based directly on the driver's SWA input. One such characteristic limit steer addition δ_c to ± 4°[22] using,

$$\delta_c = \delta_{\text{AFS}} - \delta_{sw} \tag{6}$$

The AFS actuator can be modelled by a simple first-order equation as follows,

$$\dot{\delta}_c = \frac{1}{t_s}\delta_{\text{AFS}} - \frac{1}{t_s}\delta_{sw} \tag{7}$$

Where, t_s is the DC Motor actuator time constant. The yaw rate tracking methodology control is designed to calculate the adjusting steering angles for AFS. The AFS angle δ_{AFS} is sum of additional/corrective steer angle by controller, δ_c and SWA demanded/commanded by the driver using,

$$\delta_{AFS} = \delta_{SW} + \frac{M_{z,AFS}}{a\hat{C}_{\alpha f}} \tag{8}$$

3. RIWA-EVs model and yaw moment allocation

The EV used in this paper is driven by two RIWA. The allocation law of the yaw torque is that the outside rear wheel increased the driving/braking force while the inside rear one decreased the driving/braking force at the same time. Fig. 2(a) shows the vehicle structure with two RIWA. The external yaw moment M_z is generated by the combination of longitudinal force of each rear wheel. The applied torque and speed on each rear wheels are different $T_{ml} \neq T_{mr}$ and $\omega_{Rl} \neq \omega_{Rr}$. The external yaw moment by two RIWA as illustrated in Fig. 2(b). The vehicle longitudinal velocity can represent these performances, using the vehicle longitudinal acceleration signal ($a_{x,r}$) and vehicle speed desired ($V_{x,d}$). Considering acceleration / braking pedal positions [6], the $a_{x,r}$ is defined using,

$$V_{x,d} = V_{xo} + \int_{t}^{t+t_p} a_{x,d}\,dx \tag{9}$$

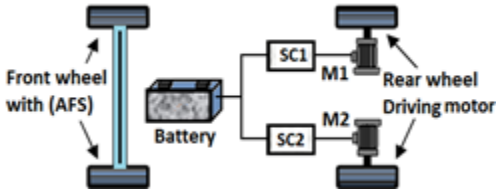

Fig. 2(a): Vehicle structure with two independent rear motors

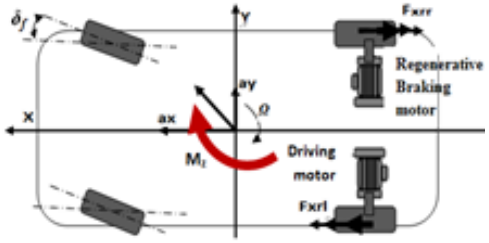

Fig. 2(b): External yaw moment by two independent rear motors

The direct yaw moment $M_{z,DYC}$ generated from independent motor traction force at each rear tire can be expressed by differential torque between the two actuators using,

$$M_{z,DYC} = \frac{T_r}{2}(F_{xrr} - F_{xrl}) - J(\dot{\omega}_{Rr} - \dot{\omega}_{Rl}) \tag{10}$$

Where Tr is the distance between the wheels of the rear axle. ωRl and ωRr are the angular acceleration. ωRl and ωRr the angular speeds of the left and right wheel drives respectively and $F_{\max,rl} = F_{Zrl}\mu$ and $F_{\max,rr} = F_{Zrr}\mu$. F_{zrl} and F_{zrr} are the vertical load of lift and right wheel of rear axle, $F_{xrl} = T_{m,l}/R_w$ and $F_{xrr} = T_{m,r}/R_w$, μ is the friction co-efficient of the tires. The difference between the two wheel velocities assures the vehicle trajectory over the curve. The wheel speed at the outer position of the curve will need to be upper than the speed of the inner wheel during curved steering [23]. The rotational velocity equations for the rear wheels are given by,

$$\begin{aligned} \frac{d\omega_{Rr}}{dt} &= \frac{T_{wr} - F_{xr}R_w}{J_w} \\ \frac{d\omega_{Rl}}{dt} &= \frac{T_{wl} - F_{xl}R_w}{J_w} \end{aligned} \tag{11}$$

Where ω_{Rr} and ω_{Rr} are the angular speed of the right and lift wheels. J_w, is the rotating inertia of the wheel. T_{wr} and T_{wl} are the torque on the right and lift wheels. F_{xr} and F_{xl} are the right and lift wheels tractive force. The linear speed of each rear wheel is defined as,

$$V_{wL} = \omega_{Rl}(R_{des} + \frac{T_r}{2}) \text{ and } \quad V_{Rr} = \omega_{Rr}(R_{des} - \frac{T_r}{2}) \tag{12}$$

Fig. 2(c) depicts a generic model of a DC motor that includes two windings. The torque of the actuator is easier to measure by using the electric motor current while the longitudinal force of each wheel is being controlled independently as follows,

$$V_b(t) = V_a(t) + R_a i_a(t) + L_a \frac{di}{dt} \tag{13}$$

$$V_b(t) = K_e \omega_m(t), \quad T_m(t) = K_1 i_a(t) \tag{14}$$

For a mechanical system undergoing pure rotational motion, an application of Newton's moment balance at the motor output shaft yields [24].

$$\begin{aligned} T_m(t) &= J_m \frac{d\omega_m(t)}{dt} + B_f \omega_m(t) + T_L(t) \\ T_m(t) &= J_m \frac{d\omega_m(t)}{dt} + B_f \omega_m(t) + J_L \frac{d\omega_m(t)}{dt} \end{aligned} \tag{15}$$

Where R_a, L_a, and K_e and K_1 are the resistance and inductance of motor winding, motor voltage constant and motor torque constant, respectively. V_b is the battery voltage, V_a is the EMF induced in the winding by the rotating rotor, T_m is the output torque, i_a is the armature current and T_L is the load torque acting on motor. ω_m is the motor angular speed. B_f is the damping co-efficient and J_m is the motor rotating inertia. The two RIWA are brushed DC motors. In order to generate DYC and achieve drive-by-wire, the two actuators should provide negative torque or positive torque for a wide range of rotational speed. The current control is achieved by properly modulating the duty cycle of the H-bridge circuit shown in Fig. 2(d).

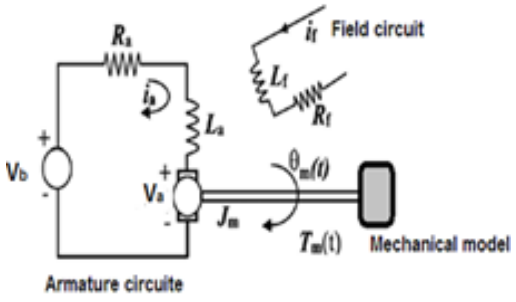

Fig. 2(c): Model of DC motor

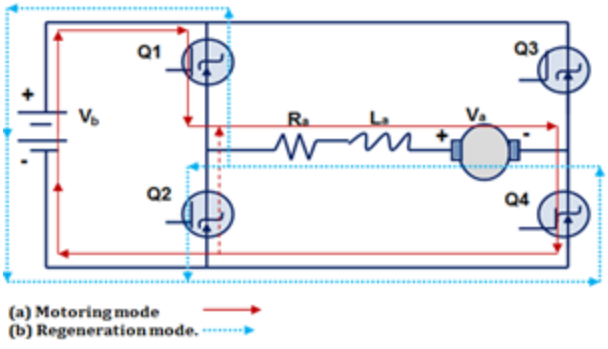

Fig. 2(d): H-bridge circuit in for motoring and forward regeneration mode

In the H-bridge circuit, Q1, Q2, Q3 and Q4 are power MOSFETs. The motor current flows clockwise in the forward motoring mode of left actuator. The right actuator is in the regeneration mode at opposite direction [6, 25]. The PWM switching on Q1 with a duty ratio Ψ is equivalent to applying a positive voltage of ΨV_b to the actuator. These equations are,

$$\psi V_b(t) = V_a(t) + R_a i_a(t) + L_a \frac{di}{dt} \quad \text{Motoring mode,} \quad i_a \geq 0 \tag{16}$$

$$(1-\psi) V_b(t) = V_a(t) + R_a i_a(t) + L_a \frac{di}{dt} \quad \text{Regeneration mode,} \quad i_a \leq 0 \tag{17}$$

4. Vehicle dynamics model

4.1. Vehicle modelling

When analysing an integrate AFS/DYC, it is essential to develop a 4-wheel vehicle dynamic model that includes tires non-linearity, longitudinal and lateral load shift, using the vehicle co-ordinate system as shown in Fig. 3(a) and the following,

$$\begin{aligned} &\text{Front, right wheel } F_{zfr} = W_f - \frac{ma_x h_{cg}}{2L} + \frac{ma_y h_{cg} b}{2T_f L} \\ &\text{Front left wheel } F_{zfl} = W_f - \frac{ma_x h_{cg}}{2L} - \frac{ma_y h_{cg} b}{2T_f L} \\ &\text{Rear right wheel } F_{zrr} = W_r + \frac{ma_x h_{cg}}{2L} + \frac{ma_y h_{cg} a}{2T_r L} \\ &\text{Rear left wheel } F_{zrl} = W_r + \frac{ma_x h_{cg}}{2L} - \frac{ma_y h_{cg} a}{2T_r L} \end{aligned} \tag{18}$$

A four-wheel model is simulated by considering the distribution of braking force, which has three degrees of freedom, i.e., longitudinal, lateral and yaw. The governing Eqns. of longitudinal and lateral motions can be expressed as follows,

$$m\dot{V}_x = ma_x = \sum F_x = F_{xfr} + F_{xfl} + F_{xrr} + F_{xrl} \tag{19}$$

$$ma_y = F_{yfr}\cos(\delta_f) + F_{yfl}\cos(\delta_f) + F_{yrr} + F_{yrl} \tag{20}$$

$$mV(\dot{\beta} + \Omega) = \sum F_y = F_{yfr} + F_{yfl} + F_{yrr} + F_{yrl} \tag{21}$$

Where m is the vehicle mass, a_x and a_y are the longitudinal and lateral vehicle accelerations, respectively and δ_f is the front steering angle. β is the vehicle slip angle, Ω is the yaw rate, F_{yfl}, F_{yfr} are the cornering forces of the front tires, F_{yrl}, F_{yrl} are the cornering forces of the rear tires, and V_x is the vehicle velocity. [26].

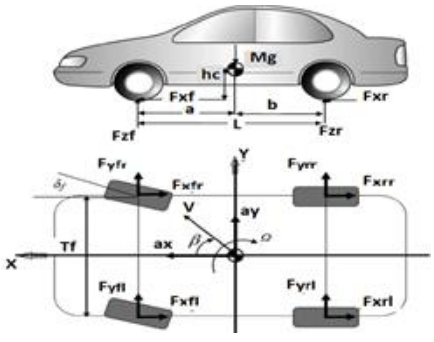

Fig. 3(a): Vehicle co-ordinates and force analysis

The yaw moment is expressed as,

$$I_z \dot{\Omega} = (F_{yfr} + F_{yfl})a - (F_{yrr} + F_{yrl})b + M_z \quad (22)$$

Where M_z is the yaw moment, which is generated by the AFS in front wheels and independent torque control of the RIWA. Under normal driving conditions, accelerations of the vehicle are low, the tire slip angles tend to be small, and the tire operates in this linear region. The tire slip angles are formulated using,

$$\begin{cases} \alpha_{fl} = -\delta_f + \arctan\left(\dfrac{V_y + a\Omega}{V_x - 0.5T_f\Omega}\right) \\ \alpha_{fr} = -\delta_f + \arctan\left(\dfrac{V_y + a\Omega}{V_x - 0.5T_f\Omega}\right) \\ \alpha_{rl} = \arctan\left(\dfrac{V_y - b\Omega}{V_x - 0.5T_f\Omega}\right) \\ \alpha_{rr} = \arctan\left(\dfrac{V_y - b\Omega}{V_x + 0.5T_f\Omega}\right) \end{cases} \quad (23)$$

When the tire operates in linear region, the lateral tire forces can be linearly approximated as follows,

$$\begin{aligned} F_{yfr} &= C_{fr}\alpha_{fr} \qquad F_{yfl} = C_{fl}\alpha_{fl} \\ F_{yrr} &= C_{rr}\alpha_{rr} \qquad F_{yrl} = C_{rl}\alpha_{rl} \end{aligned} \quad (24)$$

Where α_f and α_r are the tire slip angle for the front and rear tires, respectively. C_f and C_r are front and rear cornering stiffness. a and b are the distances of the center of gravity. I_z is the moment of inertia. To design the controller for DYC and AFS, the half vehicle model is used. A simplified two-degrees-of-freedom (2DOF) vehicle model is generally derived to describe the vehicle stability, taking the sideslip angle β and the yaw rate Ω as the states of the system, the yaw plane reference model scheme is shown in Fig. 3(b). For the simulation parameters of vehicle model as shown in Table 2, the 2DOF model can be described as,

$$\dot{\beta} = \left[-\frac{2(C_f + C_r)}{mV_x}\right]\beta + \left[-\frac{2(aC_f - bC_r)}{mV_x^2} - 1\right]\Omega + \frac{2C_f}{m}\delta_f \quad (25)$$

$$\dot{\Omega} = \left[-\frac{2(aC_f - bC_r)}{I_z V_x}\right]\beta - \left[\frac{2(a^2C_f + b^2C_r)}{I_z V_x}\right]\Omega + \frac{2aC_f}{I_z}\delta_f + \frac{M_z}{I_z} \quad (26)$$

Table 2: Main parameters of vehicle model

Parameter	Symbol	Unit	Value
Mass of the vehicle	m	kg	1200
Moment of inertia about z axis	I_z	kg.m^2	600
Wheel base	L	m	2.3
Wheel rotational inertia	J_w	kg.m^2	1.85
Distance of CG from front axle	a	m	1.035
Distance of CG from rear axle	b	m	1.265
Height of CG from ground	h_{cg}	m	0.4
Wheel radius	R_w	m	0.278
Half Track Width - front and rear axles	T_f, T_r	m	1.3
Cornering stiffness front wheels	C_f	N/rad	58000
Cornering stiffness rear wheels	C_r	N/rad	35200
Max. motor torque at speed	T_{max}/N_e	Nm/rpm	150/1400
In-wheel actuator rotational inertia	J_m	kg m^2	0.12
Gear reduction from motor to wheel	i_g	-	1

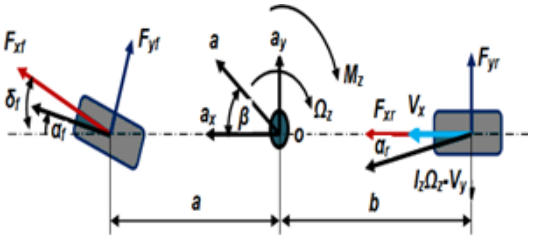

Fig. 3(b): 2-DOF yaw plane reference model

4.2. Tire model

The model of a single wheel is shown in Fig. 3(c) to obtain the actual longitudinal tire force (F_{xi}). The tire magic formula expresses the tire longitudinal force (F_{xi}), the lateral force (F_{yi}), and the aligning torque (M_{zi}) as a function of the tire side slip angle (α_i) and the longitudinal slip ratio (λ_i). The general form of the tire magic formula is as follows [27],

$$\begin{aligned} y(x) &= D\sin\left[C\tan^{-1}(Bx - E(Bx - \tan^{-1}(Bx)))\right] \\ Y(X) &= y(x + S_v) \\ x &= X + S_h \end{aligned} \quad (27)$$

Where B, C, D, and E are factors depend on the characteristics of the tire, Sh and S_v are the horizontal and vertical shifts, respectively. Y(X) is a shifted co-ordinate system to allow the generated curve by the magic formula to show an offset with respect to the origin. α is the tire slip angle, The slip ratio (λ) can be evaluated using,

$$\lambda = \frac{V_x - V_w}{V_x} = \frac{V_x - \omega.R_w}{V_x} \quad (28)$$

The wheel model undergoing perfectly straight line regenerative braking or driving manoeuvre has been considered using,

$$\begin{aligned} M_1 \ddot{X} &= F_x = \frac{T_m}{R_w} \\ J_w \dot{\omega} &= T_m - F_x.R_w \end{aligned} \quad (29)$$

Where T_m is the torque generated by the left or right motor. R_w is the radius of the wheel. $\ddot{X} = a_x$ is the vehicle acceleration. M_1 is the equivalent mass of the wheel. J_w is the inertia of wheel.

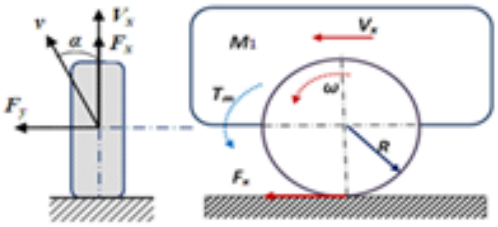

Fig. 3(c): Single wheel model

4.3. Reference model and control error calculation

The main objective in yaw rate tracking control of AFS is to bring the actual response of vehicle yaw rate close to desired response. The desired yaw rate response is determined as a function of vehicle speed V_x and front wheel steer angle δ_f in steady state condition. The

references of yaw rate and side-slip angle can be evaluated from vehicle model and operating parameters of a neutrally steered vehicle as:

$$\Omega_{des} = \frac{V}{R_{ref}} = \left[\frac{V_x}{L + K_u V_x^2}\right]\delta_f \tag{30}$$

Where k_u is known as cornering stability factor and defined as follows:

$$K_u = \frac{m(bC_r - aC_f)}{2L^2 C_r C_f} \tag{31}$$

Here, the sign of $(bC_r - aC_f)$ represents the vehicle motion behaviour by steering action. The steering characteristics are classified as follows:

$bC_r - aC_f > 0$:Under steer
$bC_r - aC_f = 0$:Neutral steer
$bC_r - aC_f < 0$:Over steer

At the same time, the maximum lateral acceleration of the vehicle is theoretically limited by the friction co-efficient of the tires using,

$$a_y \le \mu g \tag{32}$$

Where μ is the resultant friction co-efficient of the tires and g is the gravitational acceleration. In addition, the desired yaw rate is bounded by [9],

$$\Omega_{des} \le \mu \frac{g}{V_x} \tag{33}$$

To maintain lateral stability, it is important to sustain driver's control authority, which can be achieved when the vehicle sideslip angle is small [9, 28],

$$\beta_{des} = \left[\frac{1 + (maV_x^2)/(2LC_r)}{\left(1 + m\left((a/2C_r) - (b/2C_f)\right)V_x^2/(a+b^2)\right)}\right] (b/L)\delta_f \tag{34}$$

The desired sideslip angle of the vehicle is simply set to zero using,

$$\beta_{des} = 0 \tag{35}$$

According to the 2DOF model, the vehicle lateral acceleration a_y can be expressed as:

$$a_y = V_x\left[\left(\beta\frac{2(C_f + C_r)}{mV_x}\right) + \left(\Omega\frac{2(aC_f - bC_r)}{mV_x^2}\right) + \left(\frac{2C_f}{m}\delta_f\right)\right] \tag{36}$$

The reference model is assumed as the following response model which is derived by the control law of AFS on the basis of zero-sideslip in the vehicle body. As a result the yaw rate response to the steering wheel is the first order delay system. In this case, the corrective angle will be added to the outer wheel based on the error between desired and actual measured yaw rate using,

$$\Omega_{error} = \Delta\Omega = \Omega_{des} - \Omega_{act} \tag{37}$$

The error between the desired and actual measured sideslip angle is given by,

$$\beta_{error} = \Delta\beta = \beta_{des} - \beta_{act} \tag{38}$$

4.4. Driver model and vehicle path following subsystems

A dynamic path-following model is derived based on the single-track model and with the state variables in terms of position and orientation error. The configurations of the actual and desired vehicle orientations are demonstrated in Fig. 4(a). The x-y frame represents the vehicle orientation on its actual path. x_d, y_d frame represents the vehicle orientation on its desired path [27]. The predicted position is given by $\vec{R}_{Pos} = X\,\vec{i} + Y\,\vec{j}$. The predicted lateral position at preview point is given by,

$$Y(t + t_p) = Y(t) + a_y\frac{t_p^2}{2} + V_x\Omega t_p \tag{39}$$

Where, t_p denotes the driver preview time. $Y(t+t_p)$ is the predicted vehicle lateral position at the preview point, Ω is the vehicle yaw angle. The desired position vector R_d can be defined in the mobile frame *x-y* as:

$$\vec{R}_d = X_d\,\vec{i} + Y_d\,\vec{j} \tag{40}$$

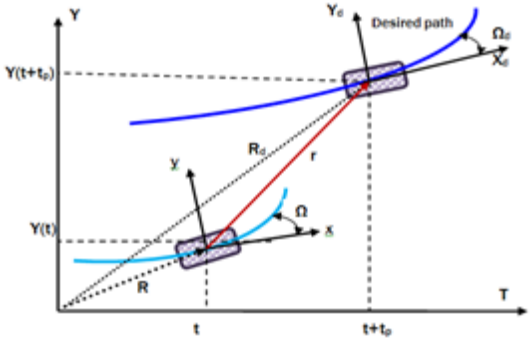

Fig. 4(a): Single point preview driver model

The goal is to minimize both the lateral position and orientation errors relative to the desired path, in order to provide a desired path control. The orientation error and its derivative can be written as follows,

$$\Delta\Omega = \Omega_{des} - \Omega_{act}$$
$$\dot{\Delta\Omega} = \dot{\Omega}_{des} - \dot{\Omega}_{act} \tag{41}$$

Where $\dot{\Omega}_{des}$ is the rate of change of the desired orientation of the vehicle and is defined as:

$$\dot{\Omega}_{des} = V_x / R_d \tag{42}$$

Where R_{des} is the radius of curvature of the desired path, the driver's control on the vehicle speed and direction of motion. To evaluate driver's control on accelerator pedal, a simple PID controller is designed to achieve the desired vehicle speed, shown in Fig. 4(b).

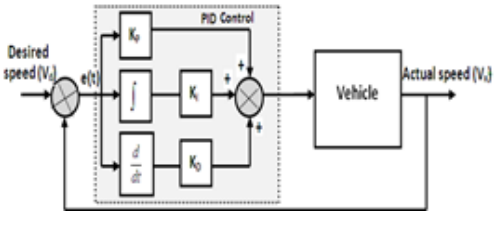

Fig. 4(b): PID controller for vehicle speed

The wheel slip controller is for the traction wheel and defined using,

$$T_{RV} = K_P e_v + K_I \int e_v dt + K_d \frac{de_v}{dt} \tag{43}$$

$$e_v = V_x - V_{x,d}$$

The controller simply provides a co-efficient for tractive torque as follows:

$$T_{RV} = K_T (T_{ml} + T_{mr}) \tag{44}$$

Where T_{RV} is the controller's commanded tractive torque. K_T is a function of the longitudinal slip of EV defined using,

$$K_T = \begin{cases} 1 & if \quad \lambda \le 0.15 \\ \dfrac{0.3-\lambda}{0.15} & if \quad 0.15 < \lambda > 0.3 \\ 0 & if \quad \lambda \ge 0.3 \end{cases} \tag{45}$$

5. Control structure design

A control strategy has been developed for vehicle DYC moment based on AFS in front axle of the vehicle together with rear wheels individual moment. The system control of the AFS/DYC vehicle stability is based on the architecture shown in Fig. 5, the scheme including the first and second controller levels. The aim of the first-level controller is to estimate the input for the second-level controller, which is given by the equivalent corrective yaw moment generated on the rear axle by individual motors $M_{z,DYC}$ and front axle by M_{z}. The first level controller is used to estimate the $M_{z,DYC}$ and $M_{z,AFS}$ for the control of vehicle stability, based on the desired vehicle behaviour, depending on the sideslip angle error $(\Delta\beta)$ and yaw rate error $(\Delta\Omega)$. The second-level controllers receive correction signals and produce the electric actuators torque, and corrected front steering angle to the vehicle. The system controller inputs are the yaw rate, angular velocity of the rear wheels, sideslip angle, steering angle, lateral position feedback and the steering wheel feed forward.

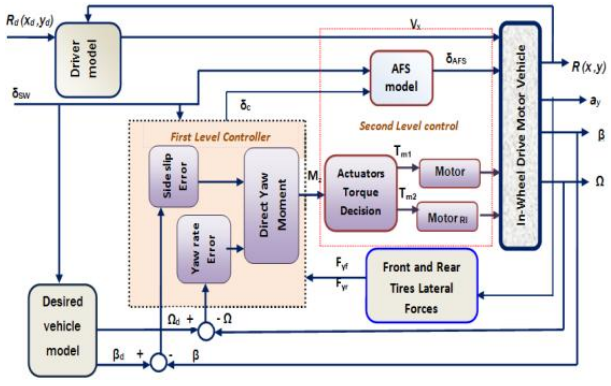

Fig. 5: Block diagram of vehicle stability control

5.1. Yaw moment controller

The objective of control system is to maintain the vehicle tracking error between the actual and desired being zero, with an optimal external yaw moment by AFS and DYC. The equivalent yaw moment generated by AFS and DYC systems are derived as,

$$M_z = M_{z,AFS} \pm M_{z,DYC} \tag{46}$$

The Linear Quadratic Regulator (LQR) theory is considered as a suitable tool for solving such problems [29-30]. The LQR methodology is used to design the vehicle stability control, the performance index used for the purpose of controller is given by,

$$J = \frac{1}{2}\int_0^{\infty} \begin{bmatrix} (\Omega - \Omega_{des})^2 + w_1(\beta - \beta_{des})^2 + \\ w_2(M_{Z,AFS}^2) + w_3(M_{Z,DYC}^2) \end{bmatrix} \tag{47}$$

Where $M_{z,AFS}$ is the correcting yaw moment by AFS depending on active front wheel steering angle, $M_{z,DYC}$ is the correcting yaw moment from rear wheels by individual in wheel motors, w_1, w_2 and w_3 are the weighting factors for balancing the relative importance of each term in the Eqn. (47)

5.2. Vehicle model for optimal controller design

The subsystem models are extended to design the optimal yaw moment controller, the linearized the 6DOF model equations obtained around steady-state trims can be written as follows,

$$\dot{x} = Ax + BU + EW \tag{48}$$

Where $X = [\Omega \quad \beta \quad \omega_{Rr} \quad \omega_{Rl} \quad \delta \quad R_{Pos}]$ and

$U = [M_{Z,AFS} \quad M_{Z,DYC}]^T$, $U = \begin{bmatrix} 0 & 0 & 0 & 0 & 1 & 0 \\ 0 & 1 & 0 & 0 & 0 & 0 \end{bmatrix}^T$,

$A = A_{(6X6)}$, $B = B_{(6X2)}$, $E = E_{(6X1)}$ and $W = [\delta_{sw}]$

The performance index Eqn. (47) is rewritten in the following form:

$$J = \frac{1}{2}\int_0^{t_f} U^T R U + \left[(X - X_d)^T Q (X - X_d)\right] dt \tag{49}$$

Where $X_d = [\Omega_d \quad \beta_d \quad 0 \quad 0 \quad 0 \quad R_d]^T$, $R = [w_1]$ and $Q = Q_{(6X6)}$. Minimization of the performance index in Eqn. (47) must be sought to improve the tracking by using minimum of the total external yaw moment. The correcting yaw moment can be considered as:

$$\begin{bmatrix} M_{Z,AFS} \\ M_{Z,DYC} \end{bmatrix} = K_\Omega \Omega + K_\beta \beta + K_{\omega Rr}\omega_{Rr} + K_{\omega Rl}\omega_{Rl} + K_\delta \delta + K_{RP} R_{Pos} + K_{sw}\delta_{sw} \tag{50}$$

Where $K_\Omega, K_\beta, K_\delta, K_{\omega Rr}, K_{\omega Rl}$ *and* K_{RP} are the feedback gains vector and K_{sw} is the feed-forward gain which must be obtained from the minimizing the cost function in Eqn. (47).

6. Experimental bench test of AFS subsystem

The overall view of the developed test rig is shown in Fig. 6(a). The test platform of the AFS system consists of the following components: Test bench, AFS controller

and motor driver, steering wheel and rack sensor and monitor program. The test bench contains the SW, column, pinion, steering rack, and the actuator. The controller is how to implement the feedback control signal to the actuator driver based on system sensors signal. The SW and column are eliminated and replaced by a side-stick in SW. The steering pinion connected with DC motor actuator has 100 W. The proposed of PID control algorithm takes the decisions based on side-stick input signals (T_d, δ_{sw}) and motor actuator is operated the RW by mechanical linkage. The control system determines the required steering angle and actuator torque based on the output as a closed loop system. The AFS responses for the FWS were measured by displacement transducer and torque sensor. The sensors signal recorded were passed to the signal processing (charge amplifier, data acquisition system, and laptop) with National Instruments LabVIEW™ program version 7.1 to create the signal recorded. The AFS installation was driven by DC motor of 100 W and selected to drive the shaft RW. The steering angle input signal, right and left rack position signals were passed to the DAC. A rack and pinion mechanism is mounted on a frame with applied simulated different spring load. Fig. 6(b) shows the, controller circuits and mounting with driver of DC motor.

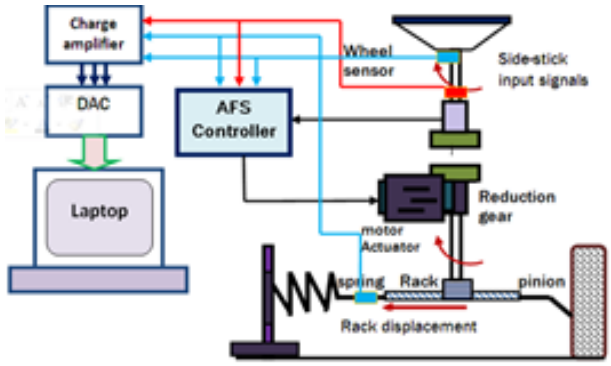

Fig. 6(a): Schematic diagram of test rig

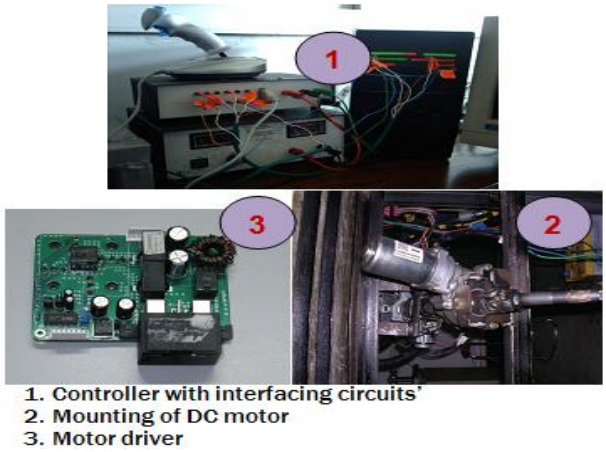

Fig. 6(b): Photographs of motor driver and control, measurement instrumentation layout

7. Results and discussions

7.1. Simulation results and analysis

For lateral (yaw) motion control, the computer simulation were conducted to evaluate the vehicle responses. The simulations are carried out for J-turn and lane change. Fig. 7 shows the characteristic curves of the lateral and longitudinal tire forces with respect to tire side slip, for various frictional road surface conditions of dry asphalt (μ=0.8), dry cobblestone (μ=0.7), wet asphalt (μ=0.4), and snow (μ=0.2), In regions of small tire slip angle (e.g., up to 4 degrees), the lateral tire forces increase linearly with respect to the increase in the slip angle and can be controlled for yaw stability enhancement by controlling the front steering angle.

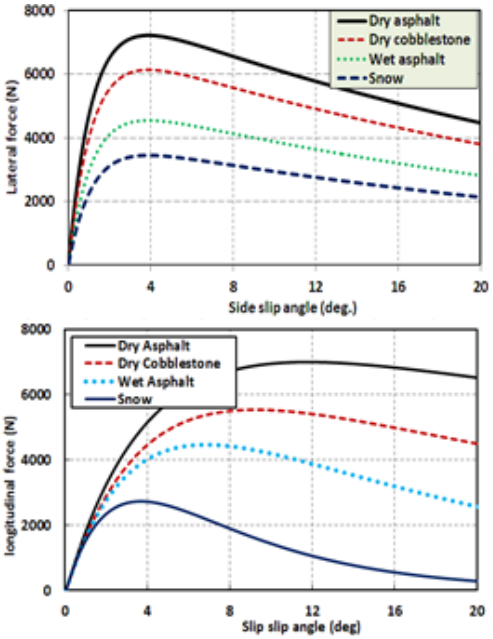

Fig. 7: Response of tire forces with various road surfaces

The first test involves road wheel angle steering input for the simulation as shown in Fig. 8(a), a J-turn is initiated by a SWA input of 700 position in 2 second and steady state on a dry road. The test result without control of vehicle model at dry asphalt road surface with different vehicle speed are processed. Fig. 8(b) shows the effect of vehicle speed on the yaw rate response, The maximum overshoot 0.235 rad/sec is 2 second of 100km/hr. The steady-state error of the system is eliminated at low speed of vehicle. Fig. 8(c) depicts the side slip angle with different vehicle speed from 30 to 100km/hr. The model shows low delay time between starting point of steering and maximum degree at vehicle speed = 30km/hr. When the vehicle speed increases to 100km/hr, the vehicle yaw and side slip exhibits high fluctuation and bounce.

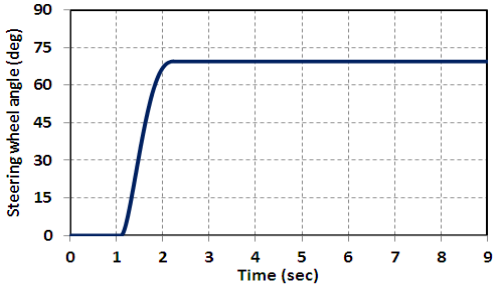

Fig. 8(a): J-turn of steering wheel angle input

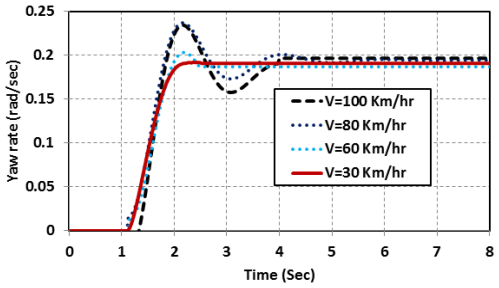

Fig. 8(b): yaw rate

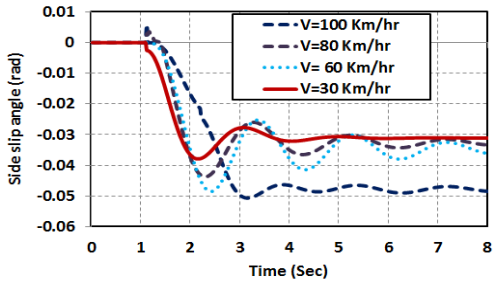

Fig. 8(c): Side slip angle

Fig. 8: Simulation results of J-turn of steering wheel angle input and response without control, μ = 0.8

The simulation results including the vehicle the yaw rate, yaw rate error, sideslip angle and lateral distance from AFS, DYC and integrated control (AFS+DYC) during the step manoeuvre at dry asphalt road μ = 0.8, v = 80km/hr are shown in Fig. 9. The yaw rate without control rapidly increases right after the steering input is applied, in vehicle stability control, when compared with the case using DYC, AFS only, the integrated control (AFS+DYC) system can improve the vehicle response and minimum side distance, which can follow the desired response. Fig. 9(d) shows clearly that the integrated control AFS+DYC can both improve the lateral displacement responsiveness and alleviate driver burden to keep the vehicle stability. The values of yaw rate and sideslip angle overshoot are decreased by 23.7% and 81.8%, respectively with integrated control (AFS+DYC). The values of yaw rate and side-slip angle transient times are decreased by 70.9% and 42.3%, respectively with integrated control (AFS/DYC). The proposed AFS/DYC is able to suppress the vehicle body side-slip angle and yaw rate and enhance stability and handing, ensuring driving comfort. The statistics of root mean square (RMS) is used in time-domain features using,

$$RMS = \sqrt{\frac{1}{N}\sum_{n=1}^{N}(x(n)-\bar{x})^2} \qquad \bar{x} = \frac{1}{N}\sum_{n=1}^{N}x(n) \qquad (51)$$

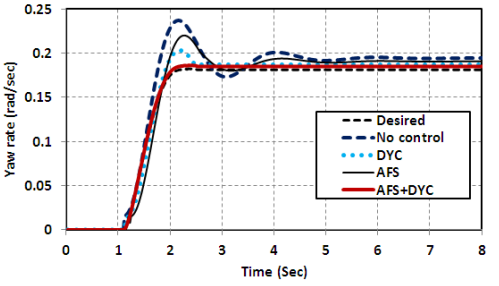

Fig. 9(a): yaw rate

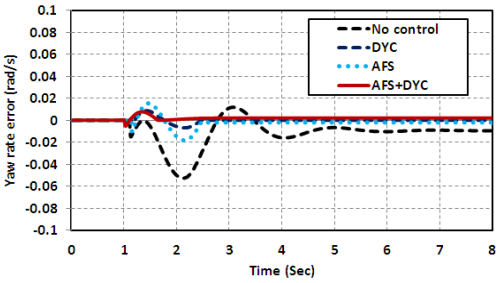

Fig. 9(b): yaw rate error

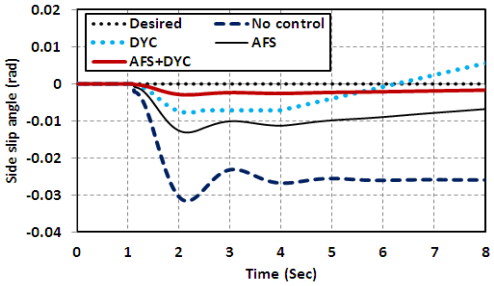

Fig. 9(c): Side-slip angle

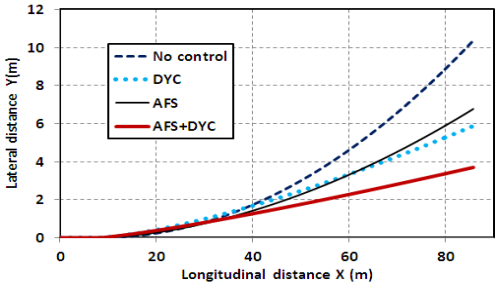

Fig. 9(d): Lateral distance

Fig. 9: The results of J-turn of SW angle input and response without control, μ = 0.8

Fig. 10(a), shows that the yaw rate was shortened approximately by 42.2% with AFS/DYC control. Fig. 10(b) shows that the reference vehicle attains an overall sideslip RMS of zero rad. This is 0.024 rad greater than the side-slip angle attained by the uncontrolled vehicle. The AFS control, the DYC control and integrated controller AFS/DYC strategies yielded respectable increases of 0.005 rad, 0.016 rad and 0.0165 rad respectively. The side-slip behaviours for the normal controller and integrated controller AFS/DYC strategies both indicate reduced body emergency during the manoeuvre [31]. Fig. 11 shows the comparison of vehicle yaw moment and steer angle of vehicle on dry road with dry asphalt road μ=0.8, v=80Km/hr. Fig. 11(a) depicts the required external yaw moment for AFS and AFS + DYC integrated controller. Fig. 11(b) depicts the corrective steer angle when applied AFS and AFS + DYC integrated controller, the maximum corrective steer angle of AFS and integrated AFS + DYC controller are 4.3° and 1.2°, respectively. Figs. 11(c) and (d) show the right and left wheel actuator torque when applied AFS and AFS + DYC integrated controller. The test of lane change according to ISO3888-1:1999 is simulated using response in Fig. 12(a) under a driver preview time 4 second, which is a short but appropriate value for an emergency situation. The desired longitudinal velocity is 80 km/h controlled by a driver model and the tire / road friction co-efficient is set as 0.8. Fig. 12(b), Fig. 12(c),

Fig. 12(d), and Fig. 12(e), illustrate the results of the yaw rate, calculated yaw rate error, vehicle sideslip, and the vehicle lateral distance, respectively. The vehicle stability can be more improved by the integrated (AFS+DYC).

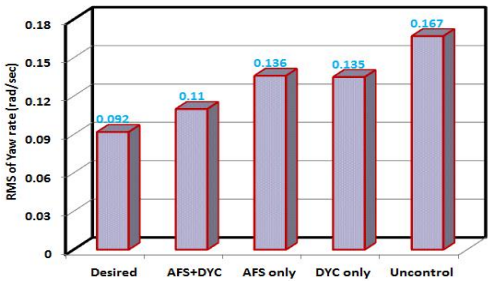

Fig. 10(a): Yaw rate comparison

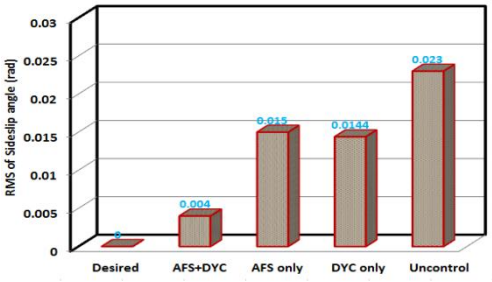

Fig. 10(b): Side-slip angle comparison

Fig. 10: Comparison of vehicle responses in a J-turn manoeuvre at dry asphalt road μ = 0.8, v = 80km/hr

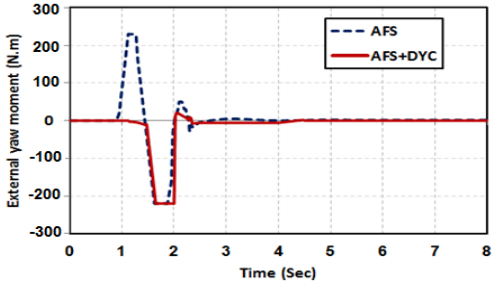

Fig. 11(a): External yaw moment

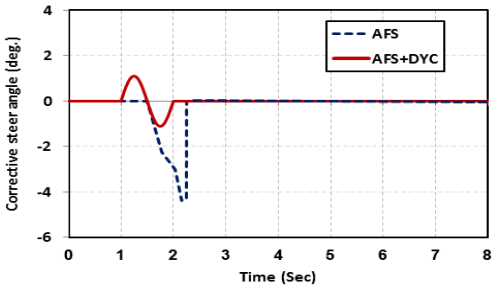

Fig. 11(b): Corrective steer angle

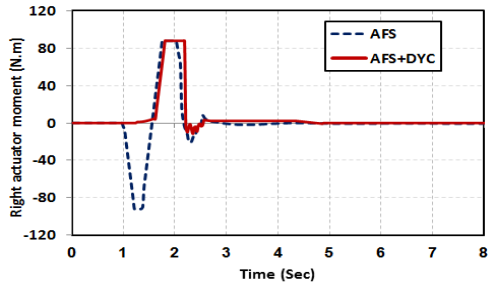

Fig. 11(c): Right actuator moment

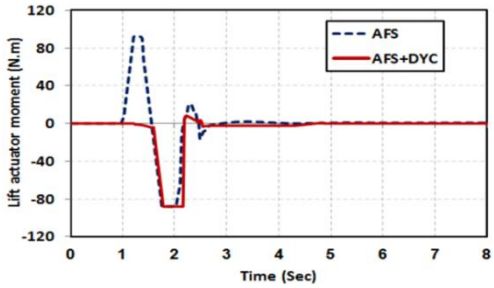

Fig. 11(d): Left actuator moment

Fig. 11: Comparison of vehicle responses moment and steer angle of vehicle on dry road with dry asphalt road μ = 0.8, v = 80km/hr

The controller rate, vehicle sideslip and lateral distance have a better convergence with integrated (AFS+DYC) controller. The magnitude of yaw rate error for the AFS + DYC integrated controller is lower than those of the other controllers and the overshot and undershot of the yaw rate has been slightly attenuated. These curves show the effectiveness of integrated controller for enhancing vehicle stability enhancement [32]. The steering ability is enhanced by the act of DYC system. As presented in Fig. 13(a), the values of the corrective external yaw moment applied by the DYC control, for the AFS or DYC individual needs the highest moment value, where integrated (AFS+DYC) needs lowest yaw moment value. Fig. 13(b) shows the applied steering torque with AFS and AFS + DYC integrated controller.

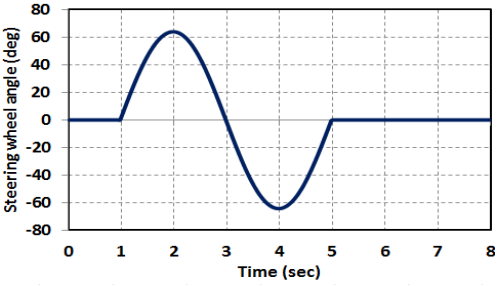

Fig. 12(a): Lane change manoeuvre of SW angle input

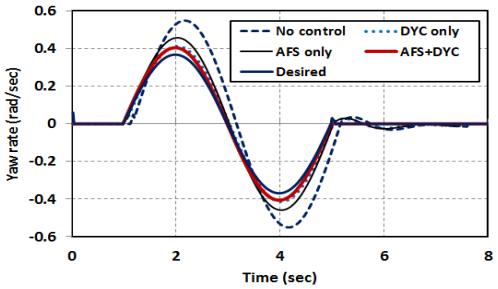

Fig. 12(b): yaw rate

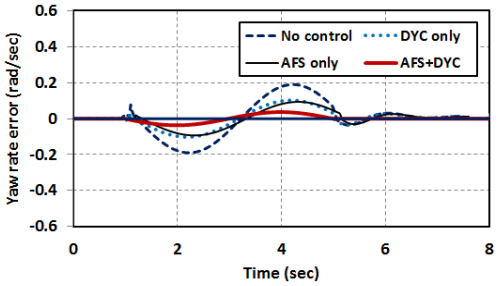

Fig. 12(c): yaw rate error

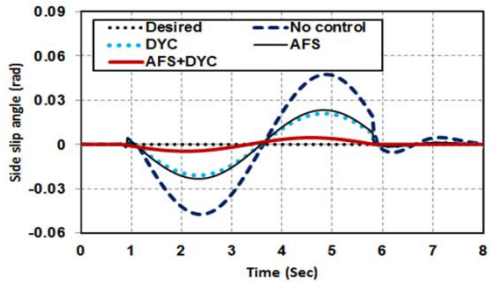

Fig. 12(d): Side-slip angle

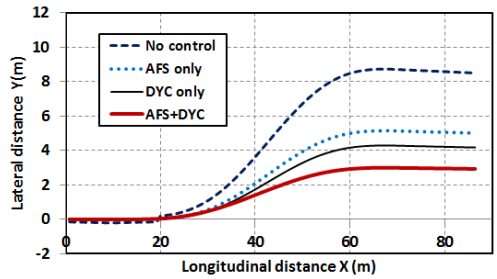

Fig. 12(e): Lateral distance

Fig. 12: Results of lane change manoeuvre, dry asphalt road μ = 0.8, v = 80km/hr

The integrated controller (AFS+DYC) needs lowest steering torque. Fig. 13(c) depicts the values of the generated moment by left and right wheel actuators of the rear axle to be applied the adjusting the vehicle yaw motion with AFS control. Fig. 13(d) depicts the values of left and right wheel actuators moment with integrated (AFS+DYC) controller. Fig. 13(e) illustrates the vehicle, left and right wheel speeds as the steering wheel moves to right. It is observed that on the rear actuator torques at the right wheel are lower than that at the left wheel, because the yaw moment is generated from vehicle tire forces to assist steering by electronic differential drive steering.

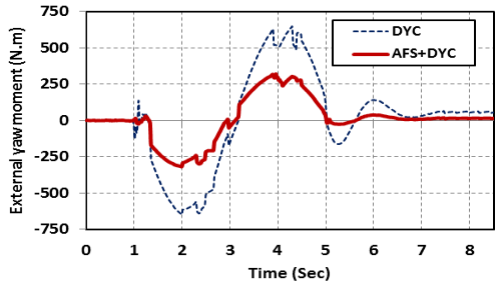

Fig. 13(a): External yaw moment

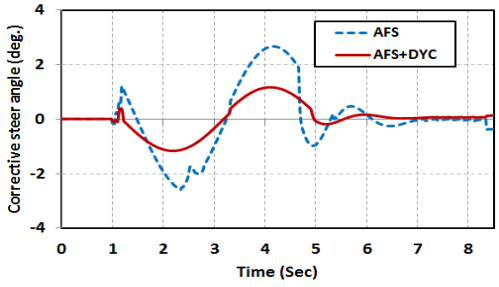

Fig. 13(b): Corrective steer angle

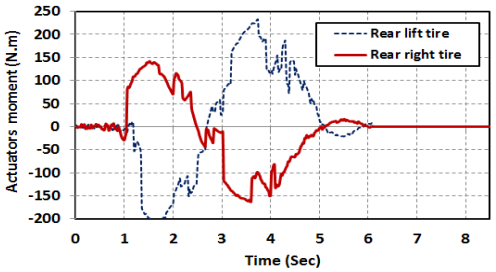

Fig. 13(c): Left and right actuators torque with AFS control

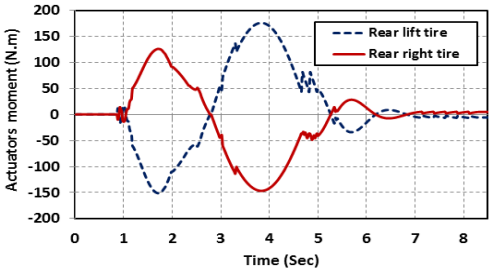

Fig. 13(d): Left and right actuators torque with AFS +DYC

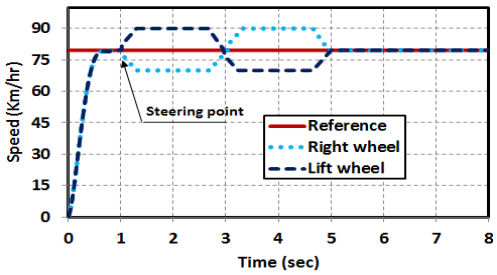

Fig. 13(e): Left and right wheels speed at turn to right direction

Fig. 13: The results for lane change manoeuvre response with μ = 0.8, v = 80Km/hr

7.2. AFS experimental and predicted results

This section presents the results obtained from the tests carried on the electronic AFS system in the laboratory. The experimental results show good agreement from 0° to 70°, according to the variation of the side-stick wheel angle SW. Note that this profile trajectory is designed to simulate the effect that the driver turns the SW for 1 sec over 8 sec. and the rack distance and RW angle can be measured by displacement sensor. Fig. 14(a) depicts the measured steering angle for SW and RW of AFS under step input. The front wheel angle compensation has a good effect on steering input. Fig. 14(b) shows the samples error in SW and RW, and shows the errors in steering SW and RW. Fig. 14(c) depicts the measured steering angle for SW and RW of AFS for lane change manoeuvre. The front wheel angle compensation has a good effect on steering. Fig. 14(d) shows the samples error in SW and RW with lane change manoeuvre input.

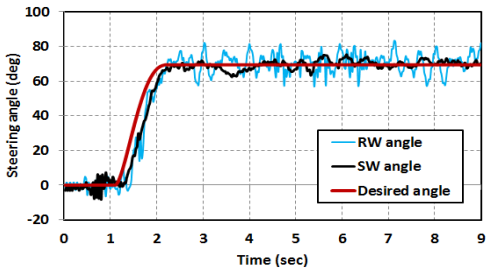

Fig. 14(a): Measured steering angle in SW and RW, for step input

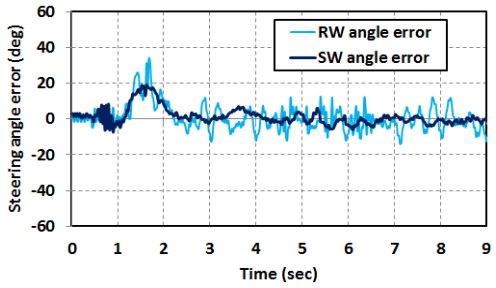

Fig. 14(b): Steering angle error, for step input

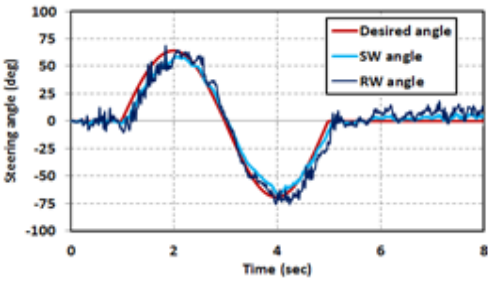

Fig. 14(c): Measured steering angle in SW and RW, for lane change manoeuvre

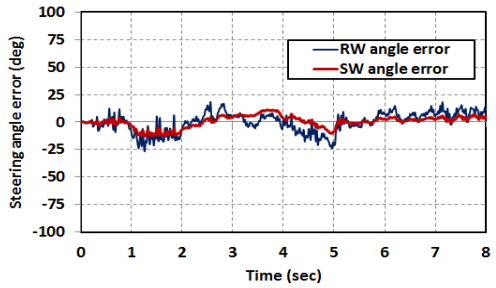

Fig. 14(d): Steering angle error, for lane change manoeuvre

Fig. 14: Measured steering angle and errors, for step and lane change manoeuvre inputs

Fig. 15 shows predictions for the yaw rate and side slip angle for step input and lane change manoeuvre of SW. Eqn. (51) is used to estimate the percentage of RMS error. Fig. 16(a) shows the percentage RMS of SW error and RW error, with different input signal. Fig. 16(b) depicts the error reductions of the yaw rate tracking error and side slip angle error. Performance improvements up to 70 % with step can be achieved when compared with a lane change manoeuvre input. Fig. 16(c) shows the measured steering DC actuator torque after adjustment, with different resistance force by using change in resistance spring stiffness 2.5, 5, 10 N/m. The DC motor current requirement increases. When the resistance force increases to 10 N/m.

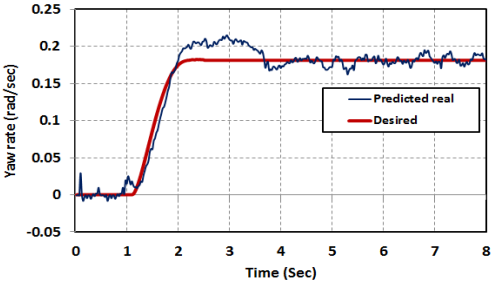

Fig. 15(a): Practical and desired yaw rate for step input

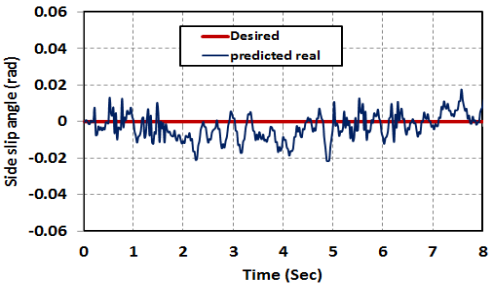

Fig. 15(b): Practical and desired side slip angle for step input

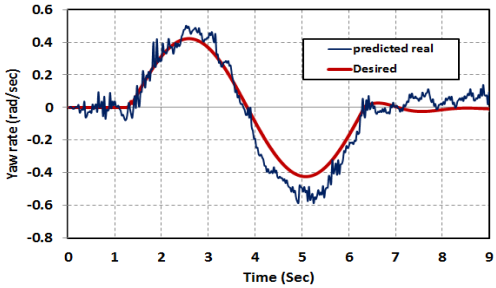

Fig. 15(c): Practical and desired yaw rate for lane change manoeuvre

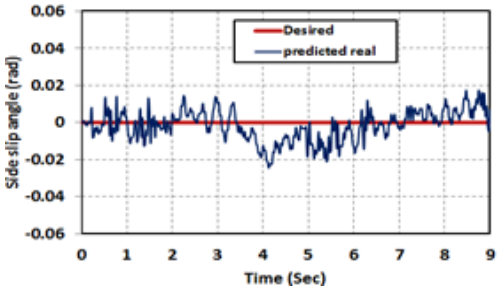

Fig. 15(d): Practical and desired side slip angle for lane change manoeuvre

Fig. 15: Practical yaw rate, yaw rate error, and side slip angle for step input

Fig. 16(d) depicts the measured DC actuator torque with different road types (concrete, dry asphalt, and wet asphalt) at constant resistance 5 N/m spring stiffness. It is also shown that the actuator torque increases with the concrete road.

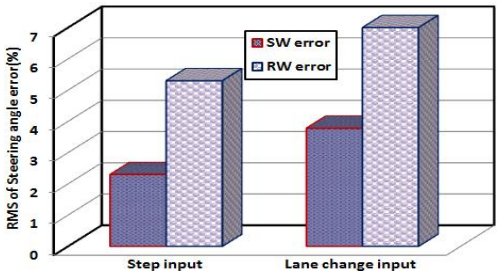

Fig. 16(a): RMS percentage of measured steering angle error

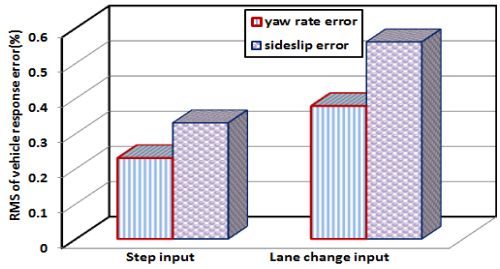

Fig. 16(b): RMS percentage of yaw rate error and sideslip

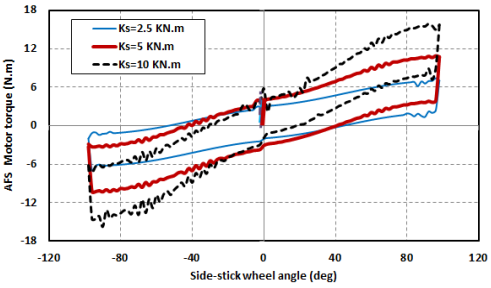

Fig. 16(c): Measured DC motor applied torque with different load spring stiffness

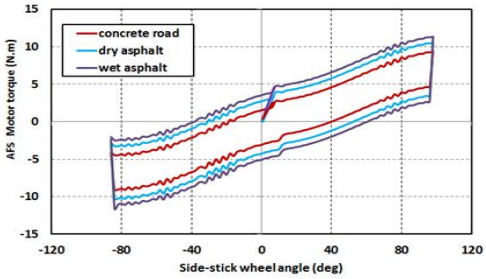

Fig. 16(d): Measured DC motor applied torque with different friction coefficient

Fig. 16: RMS of steering error and response error and measured DC motor applied torque

Fig. 17(a) shows the predicted values of the external yaw moment generated by the DYC control. When integrated (AFS+DYC) needs lowest yaw moment value to AFS. Fig. 17(b) shows the predicted steering torque with AFS and AFS + DYC integrated controller, when an integrated (AFS+DYC) needs lowest steering torque. Fig. 17(c) depicts the predicted values of the generated moment by left and right wheel actuators of the rear axle to be applied to adjust the vehicle yaw motion with AFS control. Fig. 17(d) depicts the predicted values of left and right wheel actuators moment with integrated (AFS+DYC). An integrated (AFS+DYC) is able to meet the control requirement with all the driving torques.

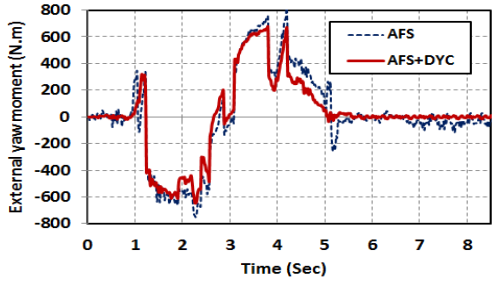

Fig. 17(a): Predicted external yaw moment

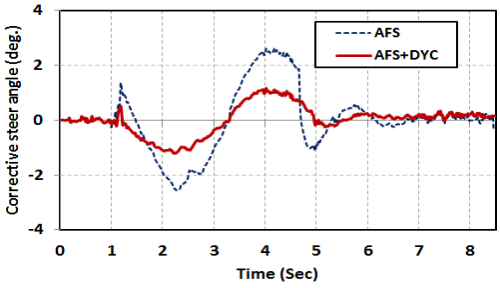

Fig. 17(b): Predicted steering torque

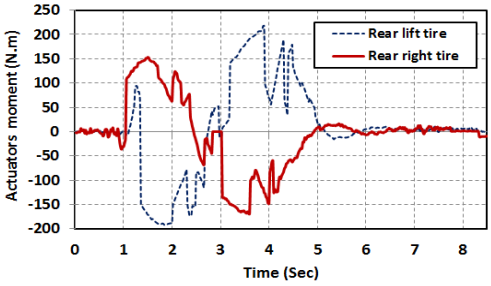

Fig. 17(c): Generated moment

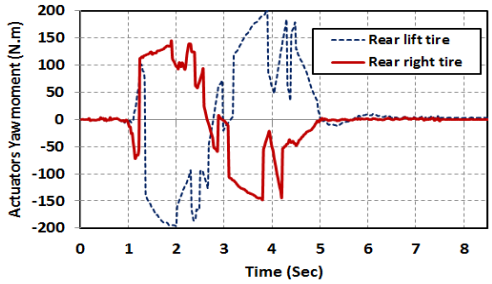

Fig. 17(d): Predicted moment

Fig. 17: Practical response for lane change manoeuvre response with dry asphalt, v = 80 km/hr and resistance 5 N/m spring stiffness

8. Conclusions

In this paper an integrated vehicle control system has been proposed to improve vehicle handling and stability, the chosen AFS and DYC by RIWA-EVs. The EVs were proved performance and stability during different road paths for varied wheel torque/speed distributions. Performance of the EVs stability control algorithm was evaluated by using MATLAB Simulink simulations. The results have shown that the vehicle with the proposed LQR stability control system, which is composed of AFS/DYC, can successfully follow the defined yaw rate and sideslip angle trajectories. This system also shows a better performance than the desired position and reduces the lateral displacement. The RMS values of yaw rate and side-slip angle overshoots are decreased by 23.7% and 81.8%, respectively with integrated AFS+DYC. Moreover, the driver assistance system by AFS/ DYC shows the effectiveness in lane-tracing performance, vehicle stability enhancement and steering effort reduction.

REFERENCES:

[1] C.C. Chan. 2007. The state of the art of electric, hybrid, and fuel cell vehicles, *Proc. IEEE*, 95(4), 704-718. https://doi.org/10.1109/JPROC.2007.892489.

[2] G.L. Solliec, A. Chasse, J.V. Frank and D. Walser. 2013. Dual mode vehicle with in-wheel motor: Regenerative braking optimization, *Oil and Gas: Sci. and Tech.*, 68(1), 95-108. https://doi.org/10.2516/ogst/2012013.

[3] K. Nam, H. Fujimoto and Y. Hori. 2014. Advanced motion control of electric vehicles based on robust lateral tire force control via active front steering, *IEEE/ASME Trans. Mechatronics*, 19(1), 289-299. https://doi.org/10.1109/TMECH.2012.2233210.

[4] G. Cong, L. Mostefai, M. Denai and Y. Hori. 2009. Direct yaw-moment control of an in wheel - motored electric vehicle based on body slip angle fuzzy observer,

IEEE Trans. Ind. Electronics, 56(5), 1411-1419. https://doi.org/10.1109/TIE.2009.2013737.

[5] H. Fujimoto, A. Tsumasaka and T. Noguchi. 2005. Direct yaw-moment control of electric vehicle based on cornering stiffness estimation, *Proc. IECON 31st Annual Conf.*, Raleigh, NC, USA.

[6] F.K. Wu, T.J. Yeh and C.F. Huang. 2013. Motor control and torque co-ordination of an electric vehicle actuated by two in-wheel motors, *Mechatronics*, 23, 46-60. https://doi.org/10.1016/j.mechatronics.2012.10.008.

[7] M. Saied and K. Damien. 2002. Vehicle handling improvement by active steering, *Vehicle System Dynamics*, 38(3), 211-242. https://doi.org/10.1076/vesd.38.3.211.8288.

[8] D. Li, S. Du and F. Yu. 2008. Integrated vehicle chassis control based on direct yaw moment, active steering and active stabilizer, *Vehicle System Dynamics*, 46, 341-351. https://doi.org/10.1080/00423110801939204.

[9] M. Nagai, M. Shino and F. Gao. 2002. Study on integrated control of active front steer angle and direct yaw moment, *JSAE Review*, 23(3), 309-315. https://doi.org/10.1016/S0389-4304(02)00189-3.

[10] Z. Shuai, H. Zhang, J. Wang, J. Li and M. Ouyang. 2014. Combined AFS and DYC control of four-wheel-independent-drive electric vehicles over CAN network with time varying delays, *IEEE Trans. Veh. Tech.*, 63(2), 591-602. https://doi.org/10.1109/TVT.2013.2279843.

[11] R. Hayama and K. Nishizaki. 2000. The vehicle stability control responsibility improvement using steer-by-wire, *Proc. IEEE Intelligent Veh. Symp.*, 596-601.

[12] S.C. Baslamisli, I.E. Kose and G. Anlas. 2009. Gain scheduled integrated active steering and differential control for vehicle handling improvement, *Vehicle System Dynamics*, 47(1), 99-119. https://doi.org/10.1080/00423110801927100.

[13] M.A. Selby, M.D. Brown, W.J. Manning and D.A. Crolla. 2001. A co-ordination approach for DYC and active front steering, *SAE Tech. Paper*, 2001-01-1275.

[14] J. Wang and R.G. Longoria. 2009. Co-ordinated and reconfigurable vehicle dynamics control, *IEEE Trans. Control Syst. Tech.*, 17(3), 723-732.

[15] H. Zhang, X. Zhang and J. Wang. 2014. Robust gain-scheduling energy-to-peak control of vehicle lateral dynamics stabilization, *Vehicle System Dynamics*, 52(3), 309-340. https://doi.org/10.1080/00423114.2013.879190.

[16] H. Du, N. Zhang and G. Dong. 2010. Stabilizing vehicle lateral dynamics with considerations of parameter uncertainties and control saturation through robust yaw control, *IEEE Trans. Vehicular Tech.*, 59(5), 2593-2597. https://doi.org/10.1109/TVT.2010.2045520.

[17] K. Kin, O. Yano and H. Urabe. 2003. Enhancements in vehicle stability and steer ability with slip control, *JSAE Review*, 24(1), 71-79. https://doi.org/10.1016/S0389-4304(02)00246-1.

[18] B. Mashadi, S. Mostaani and M. Majidi. 2011. Vehicle stability enhancement by using an active differential, *Proc. MechE., Part I: J. Systems and Control Engg.*, 225(8), 1098-1114.

[19] R. Russo, S. Strano and M. Terzo. 2016. Enhancement of vehicle dynamics via an innovative magnetorheological fluid limited slip differential, *Mechanical Systems and Signal Processing*, 70-71, 1193-1208. https://doi.org/10.1016/j.ymssp.2015.09.029.

[20] M. Abe. 1999. Vehicle dynamics and control for improving handling and active safety: from four-wheel steering to direct yaw moment control, *Proc. IMechE., Part K: J. Multi-body Dynamics*, 213(2), 87-101.

[21] S.C. Chang. 2007. Synchronization in a steer-by-wire vehicle dynamic system, *Int. J. Engg. Sci.*, 45, 628-643. https://doi.org/10.1016/j.ijengsci.2007.04.008.

[22] B. Mashadi and M. Majid. 2011. Integrated AFS/DYC sliding mode controller for a hybrid electric vehicle, *Int. J. Vehicle Design*, 56(1/2/3/4), 246-269. https://doi.org/10.1504/IJVD.2011.043268.

[23] D. Azeddine. 2013. A simplified sliding mode controlled electronic differential for an electric vehicle with two independent wheel drives, *Energy & Power Engg.*, 5(6), 416-421. https://doi.org/10.4236/epe.2013.56044.

[24] E.S. Mohamed. 2013. Design and performance analysis of the hybrid powertrain strategies for split hybrid vehicles with CVT, *Int. J. Electric and Hybrid Vehicles*, 5(3), 195-214. https://doi.org/10.1504/IJEHV.2013.057605.

[25] A. Hasan, S.Mh. Bagher and M. Sabahi. 2014. A modified integral sliding mode control to lateral stabilisation of 4-wheel independent drive electric vehicles, *Vehicle System Dynamics*, 52(12), 1584-1606. https://doi.org/10.1080/00423114.2014.951661.

[26] E.S. Mohamed and S.A. Albatlan. 2014. Analysis and testing for slip characteristics of artificial hydraulic circuit based push-belt continuously variable transmission, *Int. J. Vehicle Structures & Systems*, 6(1-2), 8-16. http://dx.doi.org/10.4273/ijvss.6.1-2.02.

[27] M. Mirzaei, G. Alizadeh, M. Eslamian and Sh. Azadi. 2008. An optimal approach to nonlinear control of vehicle yaw dynamics, *Proc. IMechE Part I: J. Systems and Control Engg.*, 222(4), 217-229.

[28] M. Behrooz, A. Pouyan, M. Majid and K. Mehdi. 2015. Integrated robust controller for vehicle path following, *Multibody System Dynamics*, 33, 207-228. https://doi.org/10.1007/s11044-014-9409-8.

[29] M. Mirzaei. 2010. A new strategy for minimum usage of external yaw moment in vehicle dynamic control system, *Transportation Research Part C*, 18, 213-224. https://doi.org/10.1016/j.trc.2009.06.002.

[30] B. Mashadi, M. Majidi and H.P. Dizaji. 2010. Optimal vehicle dynamics controller design using a four-degrees-of-freedom model, *Proc. IMechE, Part D: J. Automobile Engg.*, 224(5), 645-659.

[31] E. Esmailzadeh, A. Goodarzi and G.R. Vossoughi. 2003. Optimal yaw moment control law for improved vehicle handling, *Mechatronics*, 13, 659-675. https://doi.org/10.1016/S0957-4158(02)00036-3.

[32] S.V. Drakunov, B. Ashrafi and A. Rosiglioni. 2000. Yaw control algorithm via sliding mode control, *Proc. American Control Conf.*, 580-583.

[33] M. Boisvert and P. Micheau. 2015. Estimators of wheel slip for electric vehicles using torque and encoder measurements, *Mechanical Systems and Signal Processing*, 76-77, 665-676. https://doi.org/10.1016/j.ymssp.2016.02.017.